Published in final edited form as:
J Alzheimers Dis. 2011 ; 26(Suppl 3): 263–274. doi:10.3233/JAD-2011-0040.

Mapping the structural brain changes in Alzheimer's disease: The independent contribution of two imaging modalities

Elisa Canu, MS[1,*], **Donald G McLaren, BA**[2,3,4], **Michele E Fitzgerald, MS**[2,4], **Barbara B Bendlin, PhD**[2,4], **Giada Zoccatelli, PhD**[5], **Franco Alessandrini, MD**[5], **Francesca B Pizzini, MD, PhD**[5], **Giuseppe K Ricciardi, MD**[5], **Alberto Beltramello, MD**[5], **Sterling C Johnson, PhD**[2,4], and **Giovanni B Frisoni, MD**[1]

[1]LENITEM - Laboratory of Epidemiology Neuroimaging & Telemedicine, IRCCS Centro San Giovanni di Dio FBF, The National Centre for Research and Care of Alzheimer's and Mental Diseases, Brescia, Italy

[2]Geriatric Research Education and Clinical Center, William S. Middleton Memorial Veteran's Hospital, Madison, WI

[3]Neuroscience Training Program, University of Wisconsin, Madison, WI

[4]Wisconsin Alzheimer's Disease Research Center, Department of Medicine, University of Wisconsin, Madison

[5]Service of Neuroradiology, Ospedale Maggiore, Borgo Trento, Verona, Italy.

Abstract

The macrostructural atrophy of Alzheimer's disease (AD) has been fully described. Current literature reports that also microstructural alterations occur in AD since the early stages. However, whether the microstructural changes offer unique information independent from macrostructural atrophy is unclear. Aim of this study is to define the independent contribution of macrostructural atrophy and microstructural alterations on AD pathology.

The study involved 17 moderate to severe AD patients and 13 healthy controls. All participants underwent conventional and non conventional MRI (respectively, diffusion-weighted and T1-weighted MR scanning). We processed the images in order to obtain gray and white matter volumes to assess macrostructural atrophy, and fractional anisotropy and mean diffusivity to assess the microstructural damage. Analyses of covariance between patients and controls were performed to investigate microstructural tissue damage independent of macrostructural tissue loss, and viceversa, voxel by voxel.

We observed microstructural differences, independent of macrostructural atrophy, between patients and controls in temporal and retrosplenial regions, as well as in thalamus, corticopontine tracts, striatum and precentral gyrus. Volumetric differences, independent of microstructural alterations, were observed mainly in the entorhinal cortex, posterior cingulum, and splenium.

Measures of microstructural damage provide unique information not obtainable with volumetric mapping in regions known to be pivotal in AD as well as in others thought to be spared. This work

Corresponding author: Giovanni B Frisoni, LENITEM - Laboratory of Epidemiology, Neuroimaging & Telemedicine, IRCCS San Giovanni di Dio – FBF, Via Pilastroni 4, 25125 – Brescia, Italy, Tel: +39 0303501361, Fax: +39 02 700435727, gfrisoni@fatebenefratelli.it.
[*]current address: Neuroimaging Research Unit, Institute of Experimental Neurology, Division of Neuroscience, Scientific Institute and University Ospedale San Raffaele, Milan, Italy

All authors report no conflicts of interest.

expands the understanding of the topography of pathological changes in AD that can be captured with imaging techniques.

Keywords

Diffusion Tensor Imaging (DTI); Alzheimer's disease (AD); Microstructure; Fractional Anisotropy (FA); Mean Diffusivity (MD)

Introduction

Although Alzheimer's disease (AD) has been often described as a disease of the gray matter (GM), white matter (WM) alterations are also commonly observed [1-4] at the early stages of the disease as well as in preclinical conditions. Whether these alterations are explained by a primary WM damage, or as a degeneration secondary to GM loss (or both) is currently unknown and requires further research [5]. Microstructural investigations with diffusion tensor imaging (DTI) offer a promising approach to improve our understanding of WM, but also GM, changes in disease detection and progression [6, 7]. At the microscopic level, brain parenchymal structures have distinct boundaries, including axons membranes and myelin sheaths, which constrain the diffusion of water molecules along boundaries rather than across them [8]. Fractional anisotropy (FA) and mean diffusivity (MD) are two quantitative indices of diffusion reflecting the integrity of the brain tissue [9, 10]. Alterations in the microstructure environment, as happens in neurodegenerative processes, such as small vessel alterations, demyelination of axonal structures, degradation of microtubules, loss of axonal structure and possibly gliosis reduce directional diffusion and thus reduce FA [11-13]. Increased MD results from decreased tissue density reflecting cell loss of both neurons and glia [11, 14].

In AD, a number of studies using diffusivity indices have been carried out using specific region-of-interest (ROI) analyses [15-21] or whole brain voxel-wise methods [22-24]. However, the meaning of changes in FA or MD must be interpreted cautiously because diffusivity changes may be influenced by GM and WM atrophy [25]. For instance, although these indices are considered to be measures of tissue microstructure, it is currently unknown how they are related to WM volume [25]. Moreover, the relationship between FA and volume may not be consistent across the lifespan [26, 27], due to changes in cell and tissue complexity at different stages of development and aging [28], and this relationship may be altered further by neurodegenerative disease. Thus, the situation is more complicated in presence of tissue atrophy. A study by Hugenschmidt and colleagues [29] used a recently published method [30] to detect FA changes over WM and GM volume loss in 66 healthy adults across a broad age span. They observed that regions exhibiting decrease in FA in middle age were the same areas that exhibit volume loss in older age, suggesting that microstructural FA changes may precede and predict volume loss. They also found age-related decreases in FA in atrophy-spared regions, suggesting FA provides unique information.

Isolating the contribution of microstructural damage in AD will likely improve models of disease progression, be important for early diagnosis and for monitoring the efficacy of treatments. The purpose of the present study is to determine whether AD patients show microstructural changes that are not explained by GM and WM volume loss in areas specific to AD. In the light of previous data on healthy people [29], we hypothesized that AD patients compared to controls would exhibit separable microstructural (FA and MD indices) and macrostructural or volumetric changes (GM and WM volume loss) that each provide unique information about the disease.

Methods

Participants

Seventeen patients with moderate to severe probable AD, diagnosed according to NINCDS-ADRDA criteria [31] at the IRCCS Centro S. Giovanni di Dio Fatebenefratelli (Brescia, Italy) and 13 healthy volunteers participated in the study. The participant or primary caregiver provided written informed consent. All patients with a Clinical Dementia Rating of 2 or greater [32], were included in this study. Additionally, disease severity was assessed with the Mini Mental State Examination (MMSE) [33]. Healthy volunteers were mostly patients' non-consanguineous relatives of similar age. Exclusion criteria included history of transient ischemic attack (TIA) or stroke, WM hyperintensities and lesions, head trauma, alcohol or substance abuse, corticosteroid therapy, recent weight loss, or a modified Hachinski ischemic scale score greater than 4 [34]. Standardized history taking, behavioral and functional assessments, physical and neurological examinations, and a comprehensive neuropsychological battery were carried out for all the participants. There was no difference in age between groups, however they differed in gender, years of education and MMSE score (Table 1). The study was approved by the Ethics Committee of the Centre in accordance with the Declaration of Helsinki.

MRI acquisition

Images were acquired on a Siemens (Erlangen, Germany) 3 Tesla Allegra scanner at the Neuroradiology Unit of the Ospedale Maggiore Borgo Trento, Verona, Italy, with a standardhead coil. High resolution T1-weighted scans were acquired with a 3D sagittal magnetization prepared rapid gradient echo and diffusion-weighted images were acquired in 30 directions. These MRI sequences were acquired totally in about 12 minutes.

Imaging post-processing

T1-weighted MR and DTI images were processed in order to be perfectly aligned each other. This was necessary for running the statistical analyses where macrostructural and microstructural tissues were analyzed together voxel by voxel. Thus, in each voxel we could be able to assess macrostructural tissue differences independent from microstructural tissue differences (and viceversa) between patients and controls.

In the following session, we briefly described the procedure from the imaging processing until the imaging analyses.

Voxel-based Morphometry (VBM)

T1-weighted MR scans were processed with Statistical Parametric Mapping software http://www.fil.ion.ucl.ac.uk/spm (SPM5, University College London, London, UK) using the following supervised protocol (see also Figure 1, beginning at the top left): (i) T1-weighted images were segmented using the VBM5 toolbox [a modified version of unified VBM, http://dbm.neuro.uni-jena.de/vbm/vbm5-for-spm5/;35] to produce gray matter (GM), white matter (WM) and cerebrospinal fluid (CSF) tissues in a common space (MNI space); (ii) tissue segmentations were averaged across participants and smoothed with an 8mm FWHM Gaussian filter to create prior probability maps representative of the sample; (iii) a customized T1-weighted template was created by applying the transformations produced in step (i) to the native space T1-weighted images, averaged across participants, and smoothed with an 8 mm FWHM Gaussian filter; (iv) Original T1-weighted images were segmented a second time using the custom priors to obtain new segmentation and parameters of the common space normalization. Segmenting the images one more time with the customized T1-weighted template created at the step (iii) is critical when atrophy is present in at least one group (in this case in AD). This further step improves the segmentation since, compared

to the default template of SPM5 used at the first segmentation (i), the customized T1-weighted template is more representative of the sample. The remaining process stream uses the fast diffeomorphic image registration algorithm developed by Ashburner and colleagues as implemented in the Diffeomorphic Anatomical Registration using Exponentiated Lie Algebra (DARTEL) toolbox [36]. The parameters created in DARTEL provided a more accurate spatial normalization: they improved the alignment within subjects and benefit the alignment between modalities once the DTI images are included in the procedure. Briefly using DARTEL, (v) T1-weighted images were rigidly aligned (using the rigid –body component of the normalization parameters from step (iv)) and segmented one more time into GM and WM (using the segmentation parameters from step (iv)) and resampled to 1.5 mm isotropic voxels. vi) GM and WM segments were simultaneously coregistered using the fast diffeomorphic image registration algorithm [35]; and (vi**i**) the flow fields were then applied to the rigidly-aligned segments to warp them to the common DARTEL space and then modulated using the Jacobian determinants. Modulation scales the final GM and WM images by the amount of contraction required to warp the images to the template. The final result is GM and WM volume maps for each participant, where the total amount of GM and WM remains the same as in the original images. Note that the parameters created in DARTEL provided a more accurate spatial normalization: they improve the alignment within subjects and benefit the alignment between modalities once the DTI images are included in the procedure. Prior to the statistical computations, the images were brought back to the MNI common space according to a well defined procedure [37] and smoothed with an 8 mm FWHM Gaussian filter.

Fractional Anisotropy and Mean Diffusivity

FA and MD measures were calculated with the following procedures in FSL [http://www.fmrib.ox.ac.uk/fsl/fdt/index.html, 38]: (1) image distortions in the DTI data caused by eddy currents were corrected; (2) estimation of diffusion tensors was achieved using DTIFIT; (3) three-dimensional maps of FA and MD images were computed from the tensors from step (2).

In order to employ GM and WM volume as covariates in the analyses of the DTI measurements, it was necessary to align the FA and MD maps with the T1-weighted images normalized using DARTEL. To do this we used the following procedure (see also Graph 1, beginning at the top right): (a) the non-diffusion-weighted images were normalized to the MNI T2 template in SPM5; (b) a custom FA template was created by normalizing the FA images using the normalization parameters from step (a), averaging them and smoothing them with an 8mm FWHM Gaussian filter; (c) the custom FA template was normalized to the custom T1-weighted template (VBM step (iii)) in FLIRT [http://www.fmrib.ox.ac.uk/fsl/flirt/index.html, 39]; (d) native space FA and MD images were normalized to the custom FA template (from step (c)); (e) the normalization parameters from step (d) were multiplied by the inverse transformation parameters for the second T1-weighted segmentation (VBM step (i**v**)) and applied to both the FA and MD images; (f) FA and MD images were rigidly aligned and resampled to the same voxel size as T1 weighted images using the rigid-body component of the transformations produced in VBM step (iv); (g) warped using flow fields from DARTEL (VBM step (vi)), but not modulated. As with the VBM, the FA and MD images were brought back to the common MNI space and smoothed with an 8 mm FWHM Gaussian filter similar to the strategy employed by Hugenschmidt and colleagues [29].

Masking to exclude the CSF

To exclude the CSF contamination from the results, a mask was created based on previously published CSF levels for MD [9]. For each participant's normalized and unsmoothed MD

image, a mask of voxels with values less than 0.00283 mm2/sec (2 standard deviations below the CSF mean) was created. A group mask was computed as the intersection of all participant masks. This mask has been applied after the smoothing and used through all statistical analyses.

Statistical analysis

Voxel-wise analyses were performed in order to test for group differences on GM, WM, FA, and MD regardless of the effect of the other imaging modalities. Next, voxel-wise analyses were performed using microstructural variables as voxel-wise covariates for macrostructural (GM and WM volume) group differences. Similarly, macrostructural variables (GM and WM volume) were used as voxel-wise covariates for microstructural (FA and MD) group differences. The Biological Parametric Mapping (BPM) toolbox implemented in SPM5 [29] was used. In all analyses, statistical maps were threshold at $p<0.001$ uncorrected in at least 50 edge connected voxels and total intracranial volume (TIV) and age were included in the models as non imaging covariates. For all analyses CSF voxels were excluded by using the aforementioned mask.

Macrostructural analyses (GM and WM)

VBM analyses without imaging covariates—Two analyses of covariance (ANCOVAs) were computed in SPM5 to assess GM and WM differences between AD patients and controls. GM and WM images were added in two separated models as dependent variables with the group (AD and HC) as independent factor. This approach tests for locations where volume loss may be also affected from FA and MD microstructure alterations.

VBM analyses with imaging covariates (using Biological Parametric Mapping-BPM)—Two ANCOVAs, one for GM and the other for WM, were computed using the BPM toolbox to assess macrostructural differences between AD patients and controls. GM and WM images were entered as dependent variables in two separate models with the group (AD and HC) as independent factor. FA and MD maps were included in both models as imaging covariates. This approach tests for locations where the group (AD or control) is explaining unique variance in the volume that is not accounted for by FA or MD microstructure measures.

Microstructural analyses (FA and MD)

DTI analyses without imaging covariates—We performed two ANCOVAs to assess the differences in FA and MD between AD patients and controls without using the imaging covariates. FA and MD images were added in two separated models as dependent variables with the group (AD and HC) as independent factor.

DTI analyses with imaging covariates (using BPM)—Two ANCOVAs, one for MD and the other for FA, were computed using the BPM toolbox to assess MD and FA differences between AD patients and controls. FA and MD images were entered as dependent variables in two separate models with the group (AD and HC) as independent factor. GM and WM segmented maps were included in both models as imaging covariates. This approach tests for locations where the group (AD or control) is explaining unique variance in DTI measures that is not accounted for by volume loss.

VBM/DTI Combination

To assess the overlap in VBM and DTI group differences, we identified the total volume loss (derived from the combination of the T-maps of both GM and WM analysis without

imaging covariates) and microstructural damage (derived from the combination of the T-maps of both FA and MD analysis without imaging covariates). Thus, we created the combination map included areas with either volume loss or microstructural damage. From this map, we observed regions that had volume loss only, microstructural damage only, and volume loss with microstructural damage.

Sociodemographic analyses

ANOVA and chi-squared tests were performed to analyze the sociodemographic and clinical features (Table1).

Results

Macrostructural analyses (GM and WM)

VBM analyses without imaging covariates—The AD group showed less GM than controls in the medial temporal lobe including the hippocampi, prefrontal cortex, frontal lobe, posterior cingulate cortex and cerebellum bilaterally, and in the right parietal lobe and insula (Fig. 1, ‘warm’ colors). Additionally, the AD group showed less WM than controls in the body, genu and splenium of the corpus callosum, in the left retrosplenial region and right superior parietal lobe, posterior cingulate and prefrontal region, in the cingulum, frontal lobe, occipital and temporal lobe, and cerebellar hemispheres (Fig. 1, ‘cold’ colors). No regions showed less GM or WM in the controls compared to AD patients.

VBM analyses with imaging covariates (using BPM)—After controlling for microstructural changes with BPM we found GM atrophy in AD compared to controls in the inferior temporal lobe bilaterally and in left posterior cingulate (Fig. 1, ‘warm’ colors); in WM in the splenium of corpus callosum, in the right inferior temporal lobe, in the entorhinal region and cerebellum bilaterally (Fig. 1, ‘cold’ colors). These were regions where AD group is explaining unique variance in the volume that is not accounted for by FA or MD microstructure measures.

Microstructural analysis (MD and FA)

DTI analyses without images covariates—Using an ANCOVA without GM and WM as imaging covariates, we found that AD brains had significant higher MD compared to controls in the hippocampal and parahippocampal regions, in temporal, superior parietal and medial frontal lobe bilaterally, in the right insula, internal capsule, thalamus, posterior cingulate cortex, occipital lobe, prefrontal and frontal lobe, inferior frontal gyrus and precentral gyrus, in the left caudate nucleus and anterior internal capsule, in the cingulum and corpus callosum (Fig. 2, ‘warm’ colors).

A significant reduction in FA in AD brains was found in the anterior cingulate, caudate and parietal lobe bilaterally, in right hippocampus, cerebral peduncle, thalamus and occipital lobe, in the left putamen and medial temporal lobe (Fig. 2, ‘cold’ colors).

DTI analyses with images covariates (using BPM)—Using an ANCOVA with GM and WM volume as imaging covariates, we found that AD brains had significantly higher MD, indicating damage, in the parahippocampal regions, parietal lobe and precentral gyrus, internal capsule and caudate bilaterally, in the right thalamus, occipital lobe, in the body of cingulum and in the left medial frontal lobe including white matter tracts such as fornix, corona radiata, thalamic, corticopontine and corticospinal radiation (Fig. 2, ‘warm’ colors).

Reduced FA values, indicating damage, were found in the right cerebral peduncle and posterior limb of the internal capsule, in the thalamus and parietal lobe bilaterally, and in the

left medial temporal lobe and striatum. The following tracts pass through those regions: the anterior commissure, superior corona radiata, thalamic, cortico-pontine and corticospinal radiation (Fig. 2, 'cold' colors). These were regions where AD group is explaining unique variance in DTI measures that is not accounted for by volume loss.

No regions showed a significant decrease in MD or increase in FA in AD patients compared to controls.

VBM/DTI Combination

The combination of the VBM and the DTI results reveals regions that show both atrophy and microstructrual damage (Fig. 3, green color); however, there are regions that show microstructural damage but not significant atrophy (Fig. 3, blue color); and, finally, there are regions with atrophy but not significant microstructural changes (Fig. 3, red color).

Discussion

In the present work we differentiated microstructural damage from GM and WM volume loss in patients with moderate to severe AD. We observed atrophy-independent group differences in both MD and FA, indicative of microstructural damage beyond that explained by gross GM and WM volume loss in AD. Regions affected included the medial temporal and retrosplenial regions as well as the anterior commissure, corona radiata, internal capsule, thalamus and thalamo-cortical projections, corticopontine tracts, cerebral peduncle, striatum and precentral gyrus. Finally, volumetric differences independent of microstructural changes were observed in the entorhinal cortex, inferior temporal lobe, posterior cingulate, splenium and cerebellum.

Microstructural changes in late stage AD

In the present work, without controlling for GM and WM volume loss, we observed that our results would confirm previous findings on altered diffusion changes in AD. The comparison of FA and MD between patients and controls without GM and WM maps as imaging covariates, produced results that closely resembled other DTI studies in AD. Specifically, we observed higher MD in AD group in the hippocampi and parahippocampal regions [6, 18, 21, 23], internal capsule [23, 24], cingulum and posterior cingulate cortex [6, 23, 40], medial temporal lobe and temporal pole [16, 18, 21, 23], parietal [6, 16, 21, 23] and frontal lobe [16, 23] , including the inferior and medial frontal gyrus [23]. Confirming previous studies we observed lower anisotropy in AD compared to controls in parahippocampal regions [41, 42], putamen [43], thalamus [23, 41], cerebral peduncle [24], cingulum [22, 40, 44, 45], temporal [16, 18, 21, 24, 41, 45], frontal lobe [16, 22, 23, 41, 45] and occipital lobe [41, 45].

Using the same BPM method in a normal sample with a broad age range, a previous study [29] showed that regions with decreased FA in the middle age were the same regions that exhibit volume loss in old age. In the light of those findings, regions in our sample showing microstructural alterations in AD may be predictive of future atrophy with further disease progression. While this hypothesis can only be evaluated with longitudinal follow-up, several recent studies provide supporting evidence. First, some of the regions where we found microstructural alterations independent of macrostructural volume loss, such as internal capsule, middle cerebellar peduncle, striatum, thalamus, motor cortex (precentral region), corticopontine and talamo-cortical projections, are involved in movement control. This is consistent with the notion that advanced AD patients are more likely to show motor deficits in disease stages more severe than that of the patients in the present study [24, 46]. Second, the presence of amyloid depositions and neurofibrillar tangles has been found in the

striatum of moderate AD [47], in the primary motor cortex of severe AD [48] and in early onset AD [49, 50] which may cause white matter changes in input and output projection fibers. Third, higher iron levels, known to be associated to neurodegeneration [51, 52], have been found in the striatum of moderate AD compared to controls [53]. Moreover, pathological changes in the motor system regions have been reported in AD mainly related to the severity of the disease [54]. In the light of the mentioned literature, this study shows that changes in AD, in terms of low FA and high MD values, may suggest where the atrophy could occur during the late stages of the disease. If this is true, since it has been not proven by this study, knowledge of regions at-risk for atrophy could provide valuable insight into the optimal treatment of patients when appropriate drugs are available and for monitoring the efficacy of the treatment itself.

Regions with volume loss but not microstructural changes: Why?

Without controlling for FA and MD changes, as we expected based on several previous VBM studies (for a detailed review see [55]), we found GM volume loss in regions known to be pivotal in AD such as the hippocampus, medial temporal lobe, posterior cingulate cortex and parietal lobe. Recently, using VBM, WM volume loss has been observed in AD in regions relevant for the anatomical connection through the brain as the corpus callosum [56], the parahipppocampal areas [57] and the cingulum bundle [58], which are the same regions we observed in the present study.

Moreover, we found some regions of atrophy without significant microstrucural differences, a finding that has several possible explanations. First, the relation between gross volume and DTI indices may not be linear [59, 60]. The relationship between FA and WM differs over the life-span [26, 27]. FA is related to the microstructure of WM and only some properties may affect volume such as the degree of myelination and axonal degeneration [61]. Moreover, FA reflects a complex and dense cytoskeleton of axons composed of microtubules containing cellular organelles (mitochondria and vesicles); in general the cellular microstructure of tissue influences the overall mobility of diffusing molecules by providing different barriers (intracellular and extracellular) [8], which are in turn affected by age and AD [28]. Second, the image modalities used in this study differed in voxel resolution and this may have affected sensitivity to group differences in favor of the higher resolution T1w modality. Third, morphometry findings included regions where DTI acquistion was poor such as in the inferior temporal lobe and cerebellum where inhomogeneity artifact can result in a significant signal dropout with an echo-planar acquisition such as that used to collect the diffusion-weighted images. Future studies will benefit from the use of less suceptibility-prone sequences and higher resolution DTI acquisition protocols. The latter will also assist in detecting microstructural alterations in regions where the number of crossing fiber tracts is high, such as the centrum semiovale.

Potential issues occurring when combining different modalities

Recently, the use of the multi-modality imaging has been largely adopted in order to better understand the neurobiology of several diseases *in vivo*. However, several limitations need to be considered carefully in order to avoid misleading interpretation of the findings. First, some imaging modalities, such as DTI, are more prone to distortions and artifacts than others. Second, different imaging modalities may have different spatial resolutions (as usually occurs with DTI or functional MRI compared to T1 images). As a consequence, coregistering and normalizing different imaging modalities is one of the most common source of confound.

The pathophysiology of alterations of diffusion in AD

In AD, a number of studies suggest that diffusion changes in the WM could reflect Wallerian degeneration and be secondary to cortical pathology [62]. According to this hypothesis, the amyloid β (Aβ) deposits around the neuronal cells and/or the neurofibrillary tangles in the body of the cells lead to the degeneration of axons and myelin (secondary degeneration). However, a primary damage of WM tissue can not be excluded. In fact, Aβ deposits have been found near the vessels in the WM in AD [63] and recently it has been demonstrated that Aβ peptides are cytotoxic to oligodendrocytes in vitro [64]. A neuropathologic study [65] established the phases of Aβ deposition in AD cases. They also observed that the Aβ deposition correlated with the presence and the phases of the neurofibrillar tangles. Thus, tau may also provide a mechanism pathogenesis of white matter in AD. The role of tau has recently gained credibility for the apparently successful phase II trial of an anti-tau drug (Claude M. Wischik. “Tau aggregation inhibitor (TAI) therapy with remberTM arrests disease progression in mild and moderate Alzheimer’s disease over 50 weeks”, ICAD, Chicago 2008). Tau protein binds to the microtubules for the integrity and stabilization of the cytoskeleton and for axonal transport [66]. With the disease, the axonal cytoskeleton can be perturbated [67] and axonal transport becomes disrupted [67]. Thus, the functional failure of tau due to hyperphosphorylation may be result in changes in FA. This hypothesis is supported by data from the present study, indicating that the largest areas of alteration of diffusion map to regions known to be affected by tangle pathology [68].

Limitations

Some limitations of the present study need to be discussed. The main limitation is that the significance threshold was uncorrected for multiple comparisons and this might have led to false positive results. The sample size was small and a replication of the method in a larger sample is needed for avoiding power-related issues. Second, the two imaging modalities we used differ in resolution. Although, the images are rigid aligned each others, the original resolution could still affect the results in order of false negative/positive findings. Future studies should taking into account this possible issue. Third, groups of MCI and mild AD could add information on the progression of these microstructural alterations. Finally, the impact of these alterations requires longitudinal follow-up. The longitudinal component is critical in evaluating the hypothesis that future volume loss occurs in regions with altered diffusion which was generated by the present study.

Acknowledgments

This work has been supported by research grant 125/2004 of the Italian Ministry of Health, Ricerca Finalizzata “Malattie neurodegenerative legate all’invecchiamento: dalla patogenesi alle prospettive terapeutiche per un progetto traslazionale” and by Lundbeck Italia SpA. This study was also supported by National Institutes of Health grants AG021155 and AG000213, and by the facilities and resources at the William S. Middleton Memorial Veterans Hospital.

The authors are very grateful to Melissa Romano for her precious organizational contribution on the realization and progression of the study. Finally, we wish to thank the patients and their families for their persisting and admirable collaboration.

References

[1]. Bartzokis G, Cummings JL, Sultzer D, Henderson VW, Nuechterlein KH, Mintz J. White matter structural integrity in healthy aging adults and patients with Alzheimer disease: a magnetic resonance imaging study. Arch Neurol. 2003; 60:393–398. [PubMed: 12633151]

[2]. Bowen BC, Barker WW, Loewenstein DA, Sheldon J, Duara R. MR signal abnormalities in memory disorder and dementia. AJNR Am J Neuroradiol. 1990; 11:283–290. [PubMed: 2107712]

[3]. Scheltens P, Barkhof F, Leys D, Wolters EC, Ravid R, Kamphorst W. Histopathologic correlates of white matter changes on MRI in Alzheimer's disease and normal aging. Neurology. 1995; 45:883–888. [PubMed: 7746401]

[4]. Vermersch P, Roche J, Hamon M, Daems-Monpeurt C, Pruvo JP, Dewailly P, Petit H. White matter magnetic resonance imaging hyperintensity in Alzheimer's disease: correlations with corpus callosum atrophy. J Neurol. 1996; 243:231–234. [PubMed: 8936352]

[5]. Zhang Y, Schuff N, Du AT, Rosen HJ, Kramer JH, Gorno-Tempini ML, Miller BL, Weiner MW. White matter damage in frontotemporal dementia and Alzheimer's disease measured by diffusion MRI. Brain. 2009; 132:2579–2592. [PubMed: 19439421]

[6]. Kantarci K, Jack CR Jr. Xu YC, Campeau NG, O'Brien PC, Smith GE, Ivnik RJ, Boeve BF, Kokmen E, Tangalos EG, Petersen RC. Mild cognitive impairment and Alzheimer disease: regional diffusivity of water. Radiology. 2001; 219:101–107. [PubMed: 11274543]

[7]. Rose SE, McMahon KL, Janke AL, O'Dowd B, de Zubicaray G, Strudwick MW, Chalk JB. Diffusion indices on magnetic resonance imaging and neuropsychological performance in amnestic mild cognitive impairment. J Neurol Neurosurg Psychiatry. 2006; 77:1122–1128. [PubMed: 16754694]

[8]. Beaulieu C. The basis of anisotropic water diffusion in the nervous system - a technical review. NMR Biomed. 2002; 15:435–455. [PubMed: 12489094]

[9]. Basser PJ, Pierpaoli C. Microstructural and physiological features of tissues elucidated by quantitative-diffusion-tensor MRI. J Magn Reson B. 1996; 111:209–219. [PubMed: 8661285]

[10]. Pierpaoli C, Jezzard P, Basser PJ, Barnett A, Di Chiro G. Diffusion tensor MR imaging of the human brain. Radiology. 1996; 201:637–648. [PubMed: 8939209]

[11]. Bronge L, Bogdanovic N, Wahlund LO. Postmortem MRI and histopathology of white matter changes in Alzheimer brains. A quantitative, comparative study. Dement Geriatr Cogn Disord. 2002; 13:205–212. [PubMed: 12006730]

[12]. Englund E. Neuropathology of white matter changes in Alzheimer's disease and vascular dementia. Dement Geriatr Cogn Disord. 1998; 9(Suppl 1):6–12. [PubMed: 9716238]

[13]. Moseley M. Diffusion tensor imaging and aging - a review. NMR Biomed. 2002; 15:553–560. [PubMed: 12489101]

[14]. Kantarci K, Petersen RC, Boeve BF, Knopman DS, Weigand SD, O'Brien PC, Shiung MM, Smith GE, Ivnik RJ, Tangalos EG, Jack CR Jr. DWI predicts future progression to Alzheimer disease in amnestic mild cognitive impairment. Neurology. 2005; 64:902–904. [PubMed: 15753434]

[15]. Allen G, Barnard H, McColl R, Hester AL, Fields JA, Weiner MF, Ringe WK, Lipton AM, Brooker M, McDonald E, Rubin CD, Cullum CM. Reduced hippocampal functional connectivity in Alzheimer disease. Arch Neurol. 2007; 64:1482–1487. [PubMed: 17923631]

[16]. Bozzali M, Falini A, Franceschi M, Cercignani M, Zuffi M, Scotti G, Comi G, Filippi M. White matter damage in Alzheimer's disease assessed in vivo using diffusion tensor magnetic resonance imaging. J Neurol Neurosurg Psychiatry. 2002; 72:742–746. [PubMed: 12023417]

[17]. Choi SJ, Lim KO, Monteiro I, Reisberg B. Diffusion tensor imaging of frontal white matter microstructure in early Alzheimer's disease: a preliminary study. J Geriatr Psychiatry Neurol. 2005; 18:12–19. [PubMed: 15681623]

[18]. Hanyu H, Sakurai H, Iwamoto T, Takasaki M, Shindo H, Abe K. Diffusion-weighted MR imaging of the hippocampus and temporal white matter in Alzheimer's disease. J Neurol Sci. 1998; 156:195–200. [PubMed: 9588857]

[19]. Naggara O, Oppenheim C, Rieu D, Raoux N, Rodrigo S, Dalla Barba G, Meder JF. Diffusion tensor imaging in early Alzheimer's disease. Psychiatry Res. 2006; 146:243–249. [PubMed: 16520023]

[20]. Sandson TA, Felician O, Edelman RR, Warach S. Diffusion-weighted magnetic resonance imaging in Alzheimer's disease. Dement Geriatr Cogn Disord. 1999; 10:166–171. [PubMed: 10026392]

[21]. Fellgiebel A, Wille P, Muller MJ, Winterer G, Scheurich A, Vucurevic G, Schmidt LG, Stoeter P. Ultrastructural hippocampal and white matter alterations in mild cognitive impairment: a

diffusion tensor imaging study. Dement Geriatr Cogn Disord. 2004; 18:101–108. [PubMed: 15087585]

[22]. Medina D, DeToledo-Morrell L, Urresta F, Gabrieli JD, Moseley M, Fleischman D, Bennett DA, Leurgans S, Turner DA, Stebbins GT. White matter changes in mild cognitive impairment and AD: A diffusion tensor imaging study. Neurobiol Aging. 2006; 27:663–672. [PubMed: 16005548]

[23]. Rose SE, Janke AL, Chalk JB. Gray and white matter changes in Alzheimer's disease: a diffusion tensor imaging study. J Magn Reson Imaging. 2008; 27:20–26. [PubMed: 18050329]

[24]. Xie S, Xiao JX, Gong GL, Zang YF, Wang YH, Wu HK, Jiang XX. Voxel-based detection of white matter abnormalities in mild Alzheimer disease. Neurology. 2006; 66:1845–1849. [PubMed: 16801648]

[25]. Salat DH, Tuch DS, Hevelone ND, Fischl B, Corkin S, Rosas HD, Dale AM. Age-related changes in prefrontal white matter measured by diffusion tensor imaging. Ann N Y Acad Sci. 2005; 1064:37–49. [PubMed: 16394146]

[26]. Abe O, Yamasue H, Aoki S, Suga M, Yamada H, Kasai K, Masutani Y, Kato N, Ohtomo K. Aging in the CNS: comparison of gray/white matter volume and diffusion tensor data. Neurobiol Aging. 2008; 29:102–116. [PubMed: 17023094]

[27]. Fjell AM, Westlye LT, Greve DN, Fischl B, Benner T, van der Kouwe AJ, Salat D, Bjornerud A, Due-Tonnessen P, Walhovd KB. The relationship between diffusion tensor imaging and volumetry as measures of white matter properties. Neuroimage. 2008; 42:1654–1668. [PubMed: 18620064]

[28]. Hayakawa N, Kato H, Araki T. Age-related changes of astorocytes, oligodendrocytes and microglia in the mouse hippocampal CA1 sector. Mech Ageing Dev. 2007; 128:311–316. [PubMed: 17350671]

[29]. Hugenschmidt CE, Peiffer AM, Kraft RA, Casanova R, Deibler AR, Burdette JH, Maldjian JA, Laurienti PJ. Relating imaging indices of white matter integrity and volume in healthy older adults. Cereb Cortex. 2008; 18:433–442. [PubMed: 17575289]

[30]. Casanova R, Srikanth R, Baer A, Laurienti PJ, Burdette JH, Hayasaka S, Flowers L, Wood F, Maldjian JA. Biological parametric mapping: A statistical toolbox for multimodality brain image analysis. Neuroimage. 2007; 34:137–143. [PubMed: 17070709]

[31]. McKhann G, Drachman D, Folstein M, Katzman R, Price D, Stadlan EM. Clinical diagnosis of Alzheimer's disease: report of the NINCDS-ADRDA Work Group under the auspices of Department of Health and Human Services Task Force on Alzheimer's Disease. Neurology. 1984; 34:939–944. [PubMed: 6610841]

[32]. Morris JC. The Clinical Dementia Rating (CDR): current version and scoring rules. Neurology. 1993; 43:2412–2414. [PubMed: 8232972]

[33]. Folstein MF, Folstein SE, McHugh PR. "Mini-mental state". A practical method for grading the cognitive state of patients for the clinician. J Psychiatr Res. 1975; 12:189–198. [PubMed: 1202204]

[34]. Rosen WG, Terry RD, Fuld PA, Katzman R, Peck A. Pathological verification of ischemic score in differentiation of dementias. Ann Neurol. 1980; 7:486–488. [PubMed: 7396427]

[35]. Ashburner J, Friston KJ. Unified segmentation. Neuroimage. 2005; 26:839–851. [PubMed: 15955494]

[36]. Ashburner J. A fast diffeomorphic image registration algorithm. Neuroimage. 2007; 38:95–113. [PubMed: 17761438]

[37]. McLaren DG, Kosmatka KJ, Kastman EK, Bendlin BB, Johnson SC. Rhesus macaque brain morphometry: a methodological comparison of voxel-wise approaches. Methods. 50:157–165. [PubMed: 19883763]

[38]. Behrens TE, Woolrich MW, Jenkinson M, Johansen-Berg H, Nunes RG, Clare S, Matthews PM, Brady JM, Smith SM. Magn Reson Med. 2003:1077–1088. [PubMed: 14587019]

[39]. Jenkinson M, Smith S. A global optimisation method for robust affine registration of brain images. Med Image Anal. 2001; 5:143–156. [PubMed: 11516708]

[40]. Fellgiebel A, Muller MJ, Wille P, Dellani PR, Scheurich A, Schmidt LG, Stoeter P. Color-coded diffusion-tensor-imaging of posterior cingulate fiber tracts in mild cognitive impairment. Neurobiol Aging. 2005; 26:1193–1198. [PubMed: 15917103]

[41]. Salat DH, Tuch DS, van der Kouwe AJ, Greve DN, Pappu V, Lee SY, Hevelone ND, Zaleta AK, Growdon JH, Corkin S, Fischl B, Rosas HD. White matter pathology isolates the hippocampal formation in Alzheimer's disease. Neurobiol Aging. 2008

[42]. Zhang Y, Schuff N, Jahng GH, Bayne W, Mori S, Schad L, Mueller S, Du AT, Kramer JH, Yaffe K, Chui H, Jagust WJ, Miller BL, Weiner MW. Diffusion tensor imaging of cingulum fibers in mild cognitive impairment and Alzheimer disease. Neurology. 2007; 68:13–19. [PubMed: 17200485]

[43]. Camara E, Bodammer N, Rodriguez-Fornells A, Tempelmann C. Age-related water diffusion changes in human brain: a voxel-based approach. Neuroimage. 2007; 34:1588–1599. [PubMed: 17188516]

[44]. Rose SE, Chen F, Chalk JB, Zelaya FO, Strugnell WE, Benson M, Semple J, Doddrell DM. Loss of connectivity in Alzheimer's disease: an evaluation of white matter tract integrity with colour coded MR diffusion tensor imaging. J Neurol Neurosurg Psychiatry. 2000; 69:528–530. [PubMed: 10990518]

[45]. Teipel SJ, Stahl R, Dietrich O, Schoenberg SO, Perneczky R, Bokde AL, Reiser MF, Moller HJ, Hampel H. Multivariate network analysis of fiber tract integrity in Alzheimer's disease. Neuroimage. 2007; 34:985–995. [PubMed: 17166745]

[46]. Honig LS, Mayeux R. Natural history of Alzheimer's disease. Aging (Milano). 2001; 13:171–182. [PubMed: 11442300]

[47]. Braak H, Braak E. Alzheimer's disease: striatal amyloid deposits and neurofibrillary changes. J Neuropathol Exp Neurol. 1990; 49:215–224. [PubMed: 1692337]

[48]. Suva D, Favre I, Kraftsik R, Esteban M, Lobrinus A, Miklossy J. Primary motor cortex involvement in Alzheimer disease. J Neuropathol Exp Neurol. 1999; 58:1125–1134. [PubMed: 10560655]

[49]. Golaz J, Bouras C, Hof PR. Motor cortex involvement in presenile dementia: report of a case. J Geriatr Psychiatry Neurol. 1992; 5:85–92. [PubMed: 1590915]

[50]. Jagust WJ, Davies P, Tiller-Borcich JK, Reed BR. Focal Alzheimer's disease. Neurology. 1990; 40:14–19. [PubMed: 2296360]

[51]. Zecca L, Youdim MB, Riederer P, Connor JR, Crichton RR. Iron, brain ageing and neurodegenerative disorders. Nat Rev Neurosci. 2004; 5:863–873. [PubMed: 15496864]

[52]. Loeffler DA, Connor JR, Juneau PL, Snyder BS, Kanaley L, DeMaggio AJ, Nguyen H, Brickman CM, LeWitt PA. Transferrin and iron in normal, Alzheimer's disease, and Parkinson's disease brain regions. J Neurochem. 1995; 65:710–724. [PubMed: 7616227]

[53]. Bartzokis G, Sultzer D, Mintz J, Holt LE, Marx P, Phelan CK, Marder SR. In vivo evaluation of brain iron in Alzheimer's disease and normal subjects using MRI. Biol Psychiatry. 1994; 35:480–487. [PubMed: 8018799]

[54]. Frisoni GB, Prestia A, Rasser PE, Bonetti M, Thompson PM. In vivo mapping of incremental cortical atrophy from incipient to overt Alzheimer's disease. J Neurol. 2009

[55]. Busatto GF, Diniz BS, Zanetti MV. Voxel-based morphometry in Alzheimer's disease. Expert Rev Neurother. 2008; 8:1691–1702. [PubMed: 18986240]

[56]. Chaim TM, Duran FL, Uchida RR, Perico CA, de Castro CC, Busatto GF. Volumetric reduction of the corpus callosum in Alzheimer's disease in vivo as assessed with voxel-based morphometry. Psychiatry Res. 2007; 154:59–68. [PubMed: 17174533]

[57]. Stoub TR, deToledo-Morrell L, Stebbins GT, Leurgans S, Bennett DA, Shah RC. Hippocampal disconnection contributes to memory dysfunction in individuals at risk for Alzheimer's disease. Proc Natl Acad Sci U S A. 2006; 103:10041–10045. [PubMed: 16785436]

[58]. Villain N, Desgranges B, Viader F, de la Sayette V, Mezenge F, Landeau B, Baron JC, Eustache F, Chetelat G. Relationships between hippocampal atrophy, white matter disruption, and gray matter hypometabolism in Alzheimer's disease. J Neurosci. 2008; 28:6174–6181. [PubMed: 18550759]

[59]. Peters A, Moss MB, Sethares C. Effects of aging on myelinated nerve fibers in monkey primary visual cortex. J Comp Neurol. 2000; 419:364–376. [PubMed: 10723011]

[60]. Peters A, Sethares C. Aging and the myelinated fibers in prefrontal cortex and corpus callosum of the monkey. J Comp Neurol. 2002; 442:277–291. [PubMed: 11774342]

[61]. Wozniak JR, Lim KO. Advances in white matter imaging: a review of in vivo magnetic resonance methodologies and their applicability to the study of development and aging. Neurosci Biobehav Rev. 2006; 30:762–774. [PubMed: 16890990]

[62]. Brun A, Gustafson L, Englund E. Subcortical pathology of Alzheimer's disease. Adv Neurol. 1990; 51:73–77. [PubMed: 2294667]

[63]. Iwamoto N, Nishiyama E, Ohwada J, Arai H. Distribution of amyloid deposits in the cerebral white matter of the Alzheimer's disease brain: relationship to blood vessels. Acta Neuropathol. 1997; 93:334–340. [PubMed: 9113198]

[64]. Xu J, Chen S, Ahmed SH, Chen H, Ku G, Goldberg MP, Hsu CY. Amyloid-beta peptides are cytotoxic to oligodendrocytes. J Neurosci. 2001; 21:RC118. [PubMed: 11150354]

[65]. Thal DR, Rub U, Orantes M, Braak H. Phases of A beta-deposition in the human brain and its relevance for the development of AD. Neurology. 2002; 58:1791–1800. [PubMed: 12084879]

[66]. Higuchi M, Lee VM, Trojanowski JQ. Tau and axonopathy in neurodegenerative disorders. Neuromolecular Med. 2002; 2:131–150. [PubMed: 12428808]

[67]. Lee VM, Daughenbaugh R, Trojanowski JQ. Microtubule stabilizing drugs for the treatment of Alzheimer's disease. Neurobiol Aging. 1994; 15(Suppl 2):S87–89. [PubMed: 7700471]

[68]. Braak H, Braak E, Bohl J. Staging of Alzheimer-related cortical destruction. Eur Neurol. 1993; 33:403–408. [PubMed: 8307060]

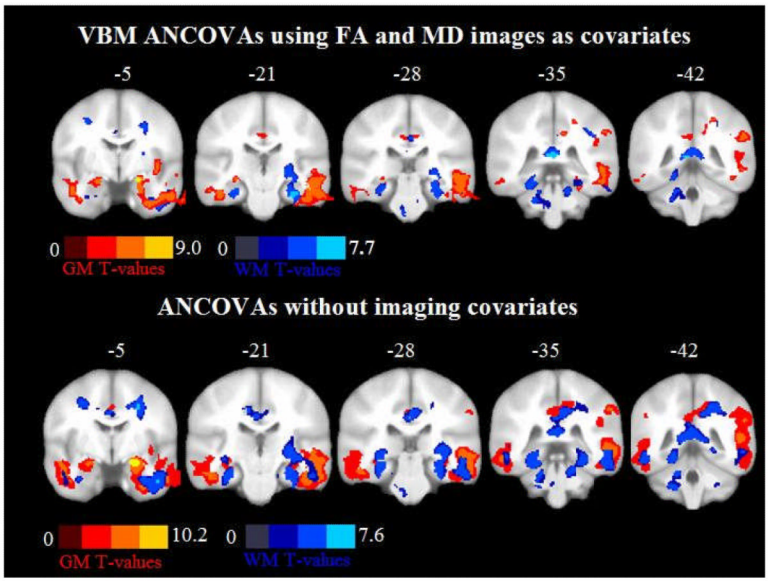

Graph 1.

A Diagrammatic Representation of the Image Processing Streams. The text provides a full description of the image processing stream with Roman Numerals detailing T1-weighted processing and letters detailing Diffusion Tensor Imaging processing. Abbreviations: T1w, T1-weighted; T2w, T2-weighted; DTI, Diffusion Tensor Imaging; S0, DTI with no diffusion weighting; MNI, Montreal Neurological Institute; DARTEL, Diffeomorphic Anatomical Registration Through Exponentiated Lie Algebra; FA, Fractional Anisotropy; MD, Mean Diffusivity; VBM5, Voxel-Based Morphometry Toolbox 5.

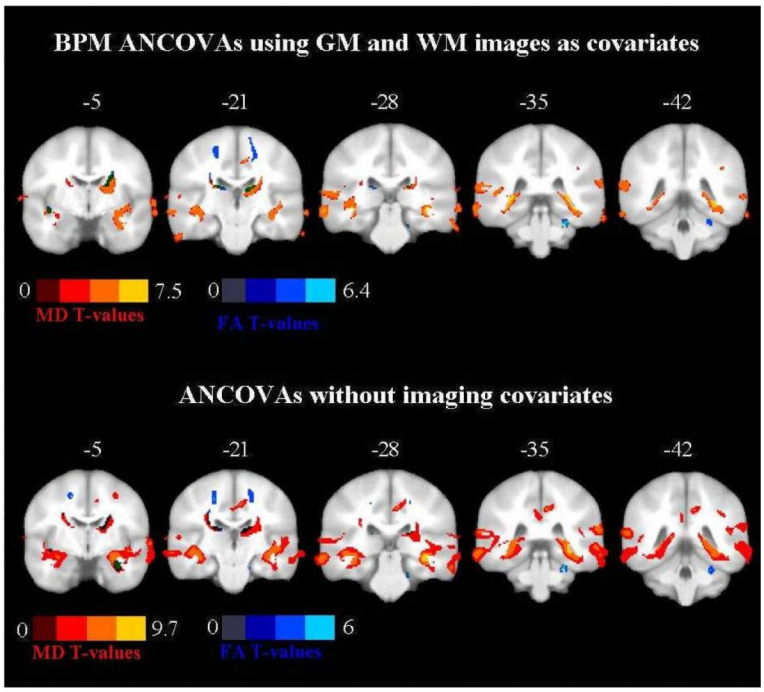

Figure 1.

Coronal slices from Y=−5 to Y=−42 showing regions with gray matter (GM, 'warm' colors) and white matter loss (WM, 'cold' colors) in Alzheimer's disease (AD) patients compared to controls. The image shows Biolgical Pattern Matching **(**BPM) analyses of covariance (ANCOVAs) using fractional anisotropy and mean diffusivity (MD) images as covariates and ANCOVAs without imaging covariates. Contrasts are shown at $p<0.001$ uncorrected in at least 50 edge connected voxels. Color bars denote t-values.

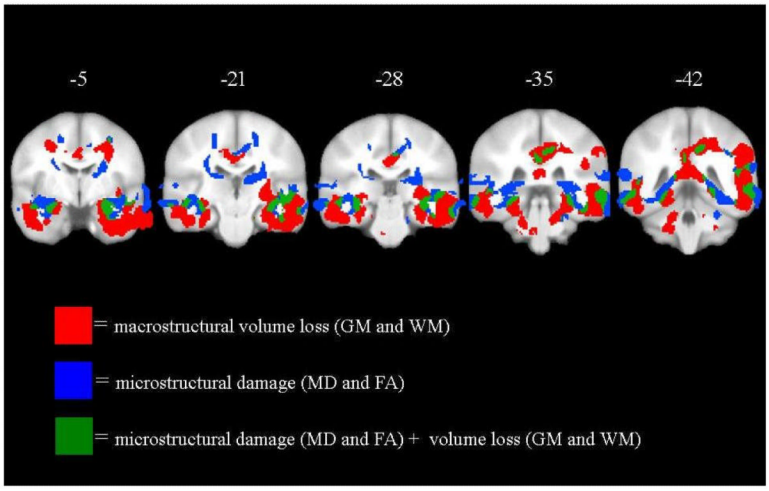

Figure 2.

Coronal slices from Y=−5 to Y=−42 showing regions with higher mean diffusivity (MD) values (’warm’ colors) and lower fractional anisotropy (FA) values (‘cold’ colors) in Alzheimer’s disease (AD) patients compared to controls. The image shows Biolgical Pattern Matching **(**BPM) analyses of covariance (ANCOVAs) using gray matter (GM) and white matter (WM) images as covariates and ANCOVAs without imaging covariates. Darkened green indicates areas with both FA and MD changes. Contrasts are shown at $p<0.001$ uncorrected in at least 50 edge connected voxels. Color bars denote t-values.

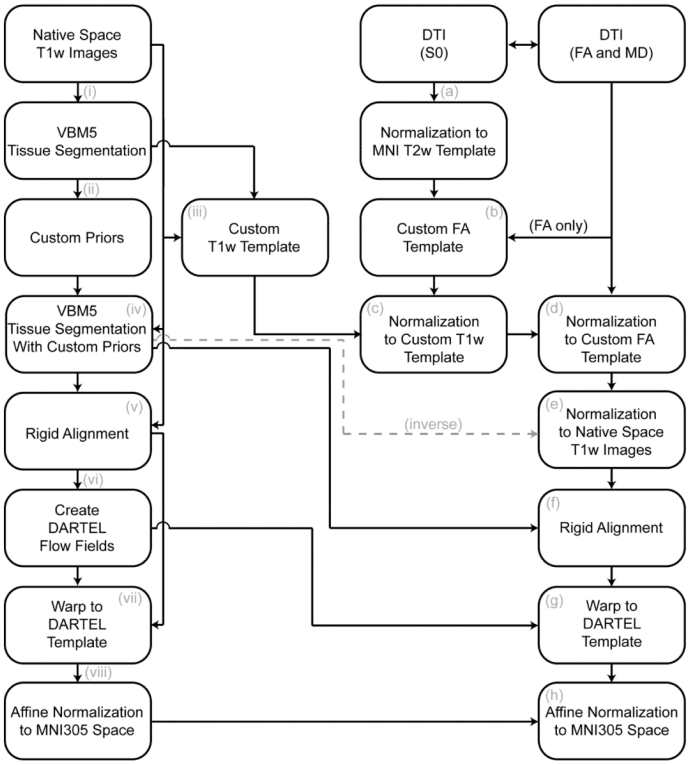

Figure 3.

Coronal slices from Y=−5 to Y=−42 showing areas with macrostructural volume loss only (gray matter-GM or white matter-WM, red); microstructural damage only (mean diffusivity-MD and fractional anisotropy-FA, blue); and the combination of macrostructural and microstructural changes (green).

Table 1

Demographic characteristics of Alzheimer's disease (AD) patients and healthy controls

	AD (n = 17)	Controls (n = 13)	*P-value*
Age, years [range]	76.7 ± 6.4 [66-87]	72.6 ± 6.6 [65-82]	.097
Gender, female	14 (82%)	6 (46%)	.038
Education, years [range]	5.5 ± 2.2 [3–13]	9.2 ± 3.2 [5-13]	.001
Mini Mental State Exam [range]	14.1 ± 3.7 [8-21]	28.9 ± 0.9 [27-30]	<.0005

Figures denote means ± SD [range] or n (%).